36th AIAA Fluid Dynamics Conference and Exhibit
5 - 8 June 2006, San Francisco, California

AIAA 2006-2867

Analysis of Flying and Swimming in Nature Using an Immersed Boundary Method

R. Mittal[*], H. Dong[†], M. Bozkurttas[‡], A. Von Loebbecke[§]
Department of Mechanical & Aerospace Engineering,
The George Washington University,
Washington, DC 20052

F.Najjar[**]
Center for Simulation of Advanced Rockets
University of Illinois at Urbana-Champaign
Urbana, IL 6180

I. Introduction

The last decade has seen a tremendous rise in the popularity of immersed boundary methods[1-6]. The primary factor driving this is the relative ease with which this methodology allows researchers to develop computational models of flows with complex geometries and/or moving boundaries. Immersed boundary solvers have been employed successfully for simulating biological flows, physiological flows, flow-induced vibration and complex turbulent flows. The key feature of the immersed boundary method is that simulations with complex boundaries can be carried out on stationary, non-body conformal Cartesian grids. This approach eliminates the need for complicated re-meshing algorithms that are usually employed with conventional Lagrangian body-conformal methods. These methods provide a unique capability for simulating flows with complex moving boundaries and as such, are ideally suited for simulation of flows associated with biological locomotion.

In the current paper, we describe a versatile immersed–boundary Cartesian grid-based method and also demonstrate the capabilities of this method for a number of biological configurations. The paper is organized as follows: in Section II, we present the numerical methodology and in Section III-V, we discuss simulation results obtained for several biologically inspired flows including the fish pectoral fin hydrodynamics, the dolphin kick in human swimmers and the aerodynamics of dragonfly flight.

II. Numerical Methodology

A finite-difference based immersed boundary methodology is used in the current simulations. As pointed out before, the key feature of these methods is that simulations with complex

[*] Associate Professor, AIAA Associate Fellow
[†] Research Scientist, AIAA Member
[‡] Graduate Student, AIAA Student Member
[§] Graduate Student, AIAA Student Member
[**] Senior Research Scientist, AIAA Senior Member

boundaries can be carried out on stationary non-body conformal Cartesian grids. Hence, this eliminates the need for complicated remeshing algorithms that are usually employed with conventional Lagrangian body-conformal methods. We solve the 3-D Navier-Stokes unsteady governing equations for a viscous incompressible flow, written in tensor form as:

$$\frac{\partial \overline{u}_i}{\partial x_i} = 0$$
$$\frac{\partial \overline{u}_i}{\partial t} + \frac{\partial \overline{u}_i \overline{u}_j}{\partial x_j} = -\frac{\partial \overline{p}}{\partial x_i} + \frac{1}{\mathrm{Re}} \frac{\partial^2 \overline{u}_i}{\partial x_j \partial x_j} - \frac{\partial \tau_{ij}^{SGS}}{\partial x_j} \qquad (1)$$

where i and j = 1, 2 and 3 correspond to x, y and z coordinates, respectively; and Re is the Reynolds number. In Equation (1), u_i is the instantaneous velocity component in the i direction, p represents the pressure, and t is the non-dimensional time. The equations have been non-dimensionalized by appropriate velocity and length scales. The solver can be run either as a DNS or an LES. In the LES formalism, the flow variables are decomposed into a large-scale (or resolved) component, denoted by overbar, and a sub-grid scale component by applying a filtering operation. Therefore, in this context, Equation (1) describes the transport of the filtered velocity field and contains the contribution of the subgrid scale (SGS) Reynolds stresses. These stresses are formulated using a Boussinesq-based eddy viscosity model and a Smagorinsky-type model is used to formulate the eddy viscosity. A dynamic Lagrangian procedure, formulated by Meneveau et al.[7] is invoked to parameterize the subgrid scale stresses.

The Navier-Stokes equations are discretized using a cell-centered collocated (non-staggered) mesh arrangement of the primitive variables (u_i, p). In addition to the cell-center velocities (u_i), the face-center velocities (U_i) are computed. In the current solution procedure, the convective terms are discretized using an explicit second-order Adams-Bashforth scheme, while the diffusive terms employ an implicit Crank-Nicolson procedure. The spatial derivatives are constructed with a second-order accurate central difference scheme. The time-integration is based on the fractional step method[8] which consists of a three-step approach. In the first step, the advection-diffusion equation is solved and the intermediate velocity, u_i^*, is obtained. In the second step, a multigrid solver is used to efficiently solve the pressure Poisson equation. This multigrid solver has been optimized to properly handle the immersed boundaries. Finally, in the third step, the cell and face-center velocity fields are updated by adding the appropriate pressure correction. At that final step, the face-velocities satisfy discrete mass-conservation to machine accuracy.

The basic concept of the current immersed boundary method is to compute the flow variables for the ghost-cells (*GC*), such that boundary conditions on the immersed boundary in the vicinity of the ghost-cells are satisfied while preserving second-order accuracy (see Figure 1 for a schematic). Ghost-cells are defined as those cells whose

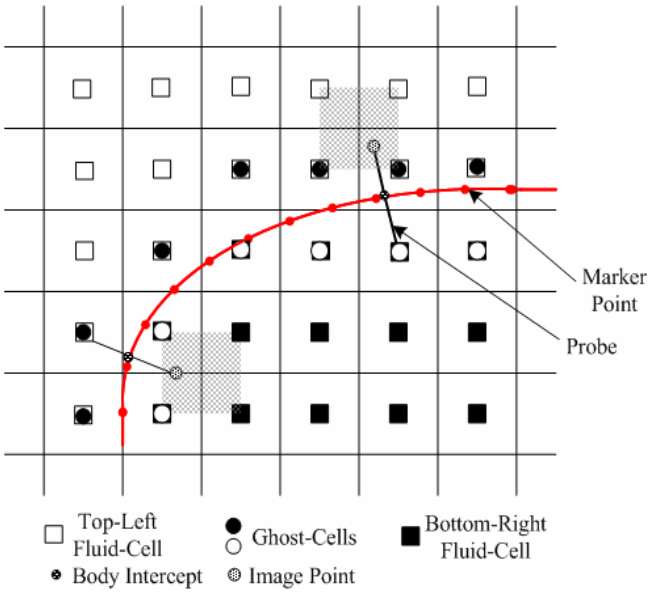

Figure 1. Designation of various nodes on the grid for membranous immersed structure.

centers lie inside the immersed body and have at least one neighboring cell which lies outside the immersed body. For an immersed membrane, the definition of ghost-cell will become more general and corresponds to those cells lying on one side of the immersed body that have at least one neighboring cells which lies on the opposite side of the immersed membrane.

The process begins by specifying the geometry of the immersed boundary. The immersed body is comprised of a surface mesh made of triangular elements and a 2D representation of this is shown in Figure 1. A non-conformal Cartesian grid is then generated followed by a procedure that identifies the ghost cells. For a membranous structure, ghost-cells are generated on both sides of the boundary. Such identification procedure is based on a robust and efficient search algorithm that begins by selecting an area around the immersed body and identifying whether these cells are solid or fluid cells. Then a fast algorithm fills the remaining computational cells with appropriate identification flag. For non-moving bodies, this procedure is performed at the start of the simulations; while for moving bodies, the procedure is invoked at every time-step.

Following the identification of the ghost cell, a probe is extended from the ghost-cells to the immersed boundary such that it intersects normal to the immersed boundary. The intersection of the probe on the immersed boundary is called the boundary intercept point (*BI*). The boundary intercept point is the location where the boundary condition will be satisfied. Next, the probe is extended further into the fluid to a distance equal to the distance between the ghost-cell and the boundary intercept point. The location at the end of the probe is referred to as the image point (*IP*). Eight cells that surround the image point are then identified and a bilinear interpolation

$$\phi_{IP} = \sum \beta_i \phi_i \tag{2}$$

is employed to calculate the value ϕ (which denote a generic variable) at the image point, where i extends over all the surrounding cells and β are the interpolated weights corresponding to the nodes surrounding the image point. All of the information regarding the local geometry of boundary and its placement relative to the mesh is incorporated into these weights (β_i). The flow variables at the ghost-cell are then computed using the value from the image point and boundary-intercept point which lay on the normal probe via a second-order interpolation. Hence for a Dirichlet and Neumann boundary conditions the values at the ghost cells are computed as follows:

$$\begin{aligned} \phi_{GC} + \phi_{IP} &= 2\phi_{BI} \\ \phi_{GC} - \phi_{IP} &= \Delta l_p \left(\frac{\delta \phi}{\delta n} \right)_{BI} \end{aligned} \tag{3}$$

For moving immersed bodies, boundary motion can be seamlessly incorporated in the current solver. To advance the governing equations from time level (n) to ($n+1$), we first move the immersed boundary from its current location to the new location by moving the vertices of the surface triangles. In the next step, the ghost-cells are identified again making use of the cells obtained from the previous timestep and the image points and body intercepts with their associated weights are recomputed. Subsequently, the governing flow equations are integrated in time using the usual time-splitting approach. Hence the current framework is considered as of Eulerian-Lagrangian nature wherein the immersed boundaries are explicitly tracked as 3D surfaces in a Lagrangian mode while the underlying flow computations are carried out on a fixed Eulerian mesh. Further details regarding the solver and immersed boundary methodology have been described in Dong et al. [6] and Bozkurttas et al.[9, 10]. In the current work, we concentrate on simulating flow past deformable fish fins, human swimmer and models of flying insects.

III. Simulation of Membranous Configurations

Simulations are performed of the flow past a flapping pectoral fin of a bluegill sunfish. The objective of this study is to examine the hydrodynamic performance and vortex topology of fish pectoral fins as a part of the research program to design maneuvering propulsor for autonomous underwater vehicles (AUV's). Fin kinematics, which was obtained from high resolution, high speed video of fish fin movement during steady swimming by a bluegill sunfish, has been provided by Lauder et.al.[11]. Surface meshes of the fin membranes have been generated based on the experimental results and included in the computations. In this set of simulations, the pectoral fin is being described as a thin membrane and flapping at a constant frequency. The key nondimensional parameters are: the Strouhal number (defined as $\mathrm{St} = L_S f / U_\infty$ where L_S, f and U_∞ are the spanwise size of the fin, fin flapping frequency and fish forward velocity, respectively) and the Reynolds number (defined as $\mathrm{Re}_\infty = U_\infty L_S / \nu$). In the current computations, the following values are used of $St = 0.54$ which matches that in the experiment and $\mathrm{Re} = 1440$, which is about one-fourth of that in the experiment.

The nominal grid size employed in the current simulations is 153 × 161 × 113, corresponding approximately to 2.78 million grid points. The mesh points have been non-uniformly distributed with an increased grid refinement near the pectoral fin membrane. A comprehensive study[12] has been carried out to assess the effect of the grid resolution and domain size on the salient features of the flow and to also demonstrate the accuracy of nominal grid size. For the present mesh resolution used here, it was clearly observed that the computed hydrodynamic forces are grid and domain independent. Table 1 shows the mean values of the hydrodynamic force coefficients produced by the fin over one flapping cycle. The force coefficient, C_F, for a given force F is computed as $C_F = F/(1/2)\rho U_\infty^2 A_{fin}$ where A_{fin} represents the nominal fin area. It is seen in Table 1 that while considerable thrust is being generated by the fin, small mean lift and spanwise force components are produced. This implies that the motion is highly efficient and allows the fish to propel itself forwards while minimizing any transverse or lateral drift.

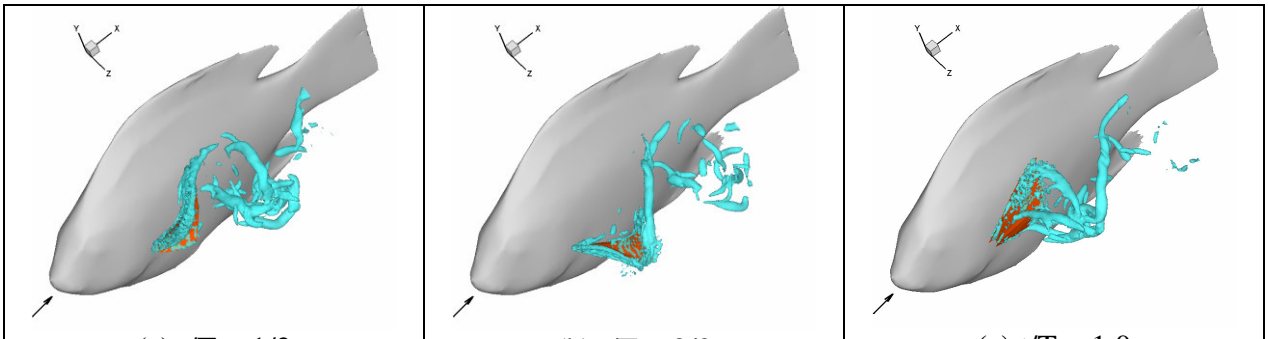

(a) t/T = 1/3 (b) t/T = 2/3 (c) t/T = 1.0

Figure 2. Wake structures for flow past a membraneous fish pectoral fin

Table 1. Mean force coefficients for flapping fin

Mean Thrust Coefficient	Mean Lift Coefficient	Mean Spanwise Force Coefficient
1.29	0.24	-0.19

Figure 2 shows the wake structures at three different time instances during the cycle where x direction is the streamwise direction, the y is vertical direction. The body of the fish is shown for viewing purpose only and is not included in the simulations. The set of three iso-surface plots shows a very complex system of vortices being generated by the fin as it moves through a typical cycle. Of particular note is the strong tip vortex observed in Figure 2(c) as well as a leading edge vortex created by the top edge of the fin both during abduction and adduction.

Lauder et.al.[11] have carried out PIV measurements of the flow past the bluegill's pectoral fin in steady swimming and these measurements have been used to validate the current simulations. The comparison between these experiments and CFD is reasonably good and provides further confidence in the fidelity of the present computational method[12].

IV. Full-Body Analysis Dolphin Kick in Swimmers

Computations are carried out of the flow past a human swimmer to investigate the dynamics of the "dolphin-kick" in competitive swimming. In this stroke, the arms and legs are stretched out and the swimmer propels him(her)self underwater by passing an undulatory wave down his(her) body. Proficiency in this stroke can give a significant competitive advantage to a swimmer since it can be used during starts and turns in freestyle, butterfly and backstroke competitions. This is a kinematically simple stroke and therefore amenable to a comprehensive analysis via CFD techniques.

In the particular video used to create motion for the current solver, the swimmer, whose outstretched body length (L) is 2.19 m, kicks at a frequency (f) of about 1.82 Hz and moves almost steadily in the water at a speed (V) of about 1.47 m/s. The toe-amplitude of the swimmer (A) is about 0.36 m and the speed (C) of the body wave can be estimated to be 1.7 m/s. Based on these, the key non-dimensional parameters are: Strouhal $(= fA/V)$ and Reynolds numbers (VL/ν) are equal to 0.45 and 3×10^6, respectively, while (A/L) and (C/V) are equal to 0.164 and 1.16, respectively. In the current simulations, we match all of these parameters except the Reynolds number which is kept at a lower value of 5×10^4. Past studies have indicated that Reynolds number plays a minor role in the flow physics of such flows and a lower Reynolds number makes these simulations more computationally feasible.

Figure 3(a) shows the body configuration of a swimmer as well as the surface mesh, which consists of around 30,000 triangles. Figures 3(b) and 3(c) presents two stages in the kick along with the vortex topology in the wake. Grids have over three million points and simulation fidelity is checked through grid refinement studies. Due to the anterior-posterior joint asymmetry in the lower limbs, the upstroke and downstroke produce different flow structures. In particular, during the upstroke, as the knees transition from flexion to extension, the ankle joint simultaneously undergoes rapid dorsiflexion from a fully plantar flexed position and this significantly increases the speed of the foot. As a result of this, each upstroke produces a remarkably well defined circular vortex ring that propagates downwards into the wake. The simulations provide a first of its kind glimpse of the fluid and vortex dynamics associated with the motions.

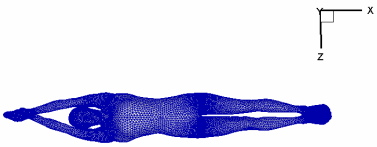

(a) Body configuration and surface mesh

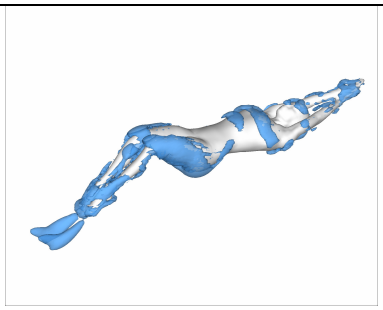

(b) t/T = 0.5

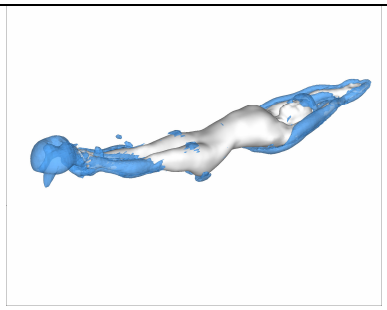

(c) t/T = 1.0

Figure 3. Simulations of dolphin-kick in competitive swimming.

V. Aerodynamics of the Dragonfly in Flight

In this section, we examine the aerodynamics of dragonfly flight with all of its complexity including the role of wing-wing interaction and wing-body interaction. To accomplish this, we have constructed a computational model of the dragonfly, referred to as Model-1 (see Figure 4a), which consists of a suitably scaled body (head, thorax and abdomen) and two pairs of flapping wings where the wings are modeled as thin ellipsoids. A grid with $128 \times 128 \times 128$ cells has been chosen for this simulation.

In this application, the motion of the each wing consists of a rotation around the root of the wing (closest point of the wing to the body) itself which is the so called the *rolling* motion. This motion of the wings can be expressed as: $\theta = A\,sin(\omega t)$, where θ defines the angle between the direction along the wing span and x- axis, $(\omega = 2\pi f)$ is the angular frequency, A is the amplitude of the motion and f is the wing beat frequency. Here the amplitudes of the motion for the wings are selected as $A = 30$ degrees (the forewings have a motion opposite to that of the hindwings). This simulation is primarily intended to show the complexity of the flow for such an insect and this is aptly demonstrated in Figure 4(b) and (c) which show the wake structures at two distinct time instances in a cycle.

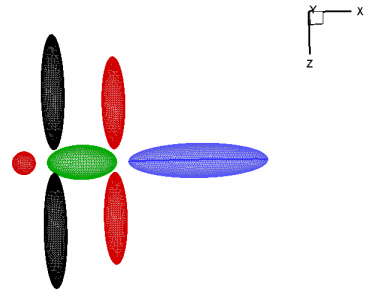

(a) Dragonfly Model-1 configuration

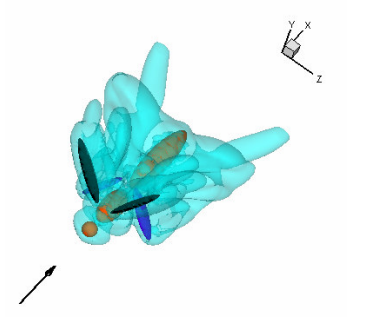

(b) t/T = 0.5

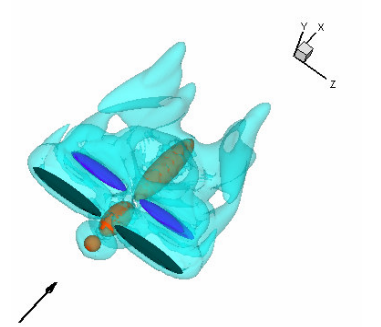

(c) t/T = 1.0

Figure 4. Simulation of a modeled dragonfly in flight.

A more realistic body configuration with membranous wings has also been created from body scan and images of a variegated meadowhawk (*Sympetrum corruptum)* which is a medium size dragonfly with a length of 33-43 mm. Some simplifications in the geometry of the body have been made to make it more suitable for CFD simulations. Figure 5(a) shows the body configuration as well as the surface mesh for Model-2 from two different perspectives. This configuration is first simulated with stationary wings at a 5 degrees angle of attack and results from this simulation are shown in Figure 5(b). In another simulation, the two set of wings are moved with the rolling motion specified for Model-1 above and figure 5(c) shows the vortex structure results from this simulation.

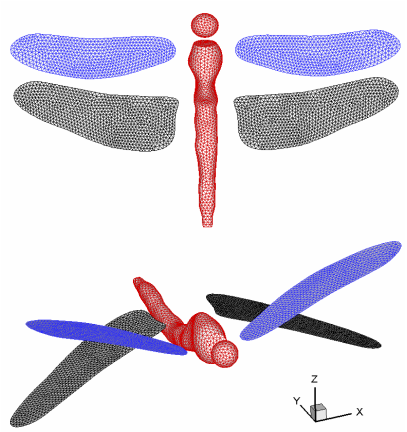

(a) Dragonfly Model-2 configuration

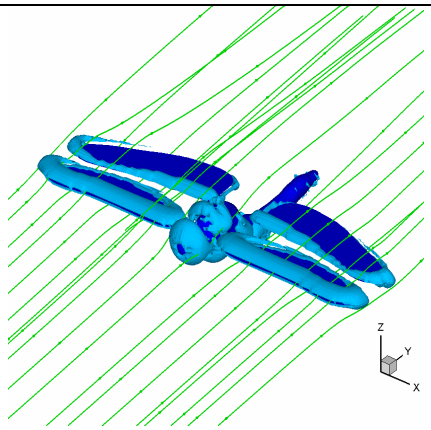

(b) Vortex structure and streamlines at 5 deg. AOA stationary case

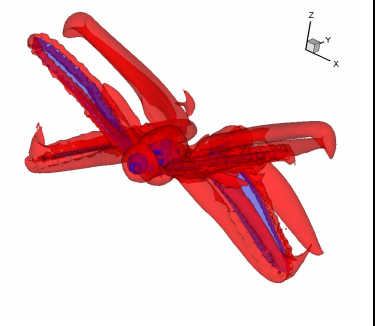

(c) t/T = 0.25

Figure 5. Simulation of a dragonfly in flight.

It should be noted that the rolling motion is selected because of its simplicity. Actual kinematic data of dragonflies in free-flight including, rolling amplitude, pitch variation, inclination of the stroke-planes, wing beat frequency and phase-relation between the fore- and hindwings, etc., have been measured[13,14] and our plan is to incorporate these in the next set of simulations.

Acknowledgment

This is work is supported under ONR-MURI Grant N00014-03-1-0897 and a grant from USA Swimming. We would also like to acknowledge discussion and collaboration with George Lauder and Peter Madden of Harvard University.

References

[1]Mittal, R., Iaccarino, G., "Immersed Boundary Methods," *Annu. Rev. of Fluid Mech.*, 2005, 37:239-61.

[2]Ye, T., Mittal, R., Udaykumar, H. S., Shyy, W., "An accurate Cartesian grid method for viscous incompressible flows with complex immersed boundaries, " *J. Comput. Phys.,* 1999, 156:209–40.

[3]Udaykumar, H. S., Mittal, R., Shyy, W., "Computation of solid-liquid phase fronts in the sharp interface limit on fixed grids," *J. Comput. Phys. ,* 1999, 153:534–74.

[4]Tran, L., Udaykumar, H. S., "A particle level set based sharp interface Cartesian grid method for impact, penetration and void collapse," *J. Comp. Phys.,*2004, 193:469–510.

[5] Peskin, C.S., "The fluid dynamics of heart valves: experimental, theoretical and computational methods," *Annu. Rev. Fluid Mech.,* 1981, 14: 235-59.

[6]Dong, H., Mittal, R., Najjar. F., "Wake Topology and Hydrodynamic Performance of Low Aspect-Ratio Flapping Foils," accepted by *J. Fluid Mechanics*, 2006.

[7]Meneveau, C., Lund, T.S., and Cabot, W.H., "A Lagrangian dynamic subgrid-scale model of turbulence," *J. Fluid Mechanics*, Vol. 319, 1996, pp. 353-385,.

[8]Chorin, A.J., "A Numerical Method for Solving Incompressible Viscous Flow Problems," *J. Comp. Phys.*, Vol. 2, 1967.

[9]Bozkurttas, M., Dong H., Seshadri V., Mittal R., Najjar F.,"Towards numerical simulation of flapping foils on fixed Cartesian grids," *AIAA 2005-0079*, Reno, NV, 2005.

[10]Bozkurttas, M., Dong, H., Mittal, R., Madden, P., Lauder, G., and Najjar, F., "Simulation of flow past flapping foils with active chordwise deformation," *AIAC 2005-034, Ankara International Aerospace Conference*, METU, TURKIYE, 2005.

[11]Lauder, G., Madden, P., Hunter, I., Tangorra, J., Davidson, N., Proctor, L., Mittal, R., Dong, H., Bozkurttas, M., "Design and Performance of a Fish Fin-Like Propulsor for AUVs", *Proceedings of 14th International Symposium on Unmanned Untethered Submersible Technology (UUST)*, Durham, New Hampshire, 2005.

[12]Bozkurttas, M, Dong, H., Mittal, R., Madden, P., Lauder, G., "Hydrodynamic performance of deformable fish fins and flapping foils," *AIAA 2006-1392*, Reno, NV, 2006.

[13]Norberg, R. A., "Hovering flight of the dragonfly *Aeschna juncea* L.,kinematics and aerodynamics," *In Swimming and Flying in Nature,* (ed. T. Y. Wu,C. J. Brokaw and C. Brennen), pp. 763-781. NewYork: Plenum Press, 1975.

[14]Wakeling, J.M. and Ellington, C.P.,"Dragonfly flight, (2). velocities, accelerations and kinematics of flapping flight," *J. Exp. Biol.* 200,1997, pp. 557-582.